Article

Acid-activatable theranostic unimolecular micelles composed of amphiphilic star-like polymeric prodrug with high drug loading for enhanced cancer therapy

Xiaoxiao Shi, Meili Hou, Shuang Bai, Xiaoqian Ma, Yong-E Gao, Bo Xiao, Peng Xue, Yuejun Kang, Zhigang Xu, and Chang Ming Li

Mol. Pharmaceutics, **Just Accepted Manuscript** • DOI: 10.1021/acs.molpharmaceut.7b00704 • Publication Date (Web): 05 Oct 2017

Acid-activatable theranostic unimolecular micelles composed of amphiphilic star-like polymeric prodrug with high drug loading for enhanced cancer therapy

Xiaoxiao Shi[a, b], Meili Hou[a, b], Shuang Bai[a, b], Xiaoqian Ma[a, b], Yong-E Gao[a, b], Bo Xiao[a, c], Peng Xue[a, b], Yuejun Kang[a, b], Zhigang Xu*[a, b] and Chang Ming Li[a, b]*

[a]Institute for Clean Energy and Advanced Materials, Faculty of Materials and Energy, Southwest University, Chongqing 400715, P. R. China

[b]Chongqing Engineering Research Centre for Micro-Nano Biomedical Materials and Devices, Chongqing 400715, P.R. China.

[c]Institute for Biomedical Sciences, Center for Diagnostics and Therapeutics, Georgia State University, Atlanta, GA 30302, USA.

Z. Xu (zgxu@swu.edu.cn); Fax: +86-68253204; Tel: +86-68253792

Y. Kang (yjkang@swu.edu.cn); Fax: +86-68253204; Tel: +86-68254056

ABSTRACT

Stimuli-responsive nanomedicine with theranostic functionalities while reduced side-effects has attracted growing attention, although there are some major obstacles to overcome before clinical applications. Herein, we present an acid-activatable theranostic unimolecular micelles based on amphiphilic star-like polymeric prodrug to systematically address typical existing issues. This smart polymeric prodrug has a preferable size of about 35 nm and strong micellar stability in aqueous solution, which is beneficial to long-term blood circulation and efficient extravasation from tumoral vessels. Remarkably, the polymeric prodrug has a high drug loading rate up to 53.1 wt %, which induces considerably higher cytotoxicity against tumor cells (HeLa cells and MCF-7 cells) than normal cells (HUVEC cells) suggesting a spontaneous tumor-specific targeting capability. Moreover, the polymeric prodrug can serve as a fluorescent nanoprobe activated by the acidic microenvironment in tumor cells, which can be used as a promising platform for tumor diagnosis. The superior anti-tumor effect in this *in vitro* study demonstrates the potential of this prodrug as a promising platform for drug delivery and cancer therapy.

KEYWORDS:

Acid-activatable; polymeric prodrug; unimolecular micelles; drug delivery, cancer therapy

INTRODUCTION

Cancer has been a prevailing threat to human health owing to high mortality and severe incidence.[1-2] Nanomedicine as a powerful therapeutic strategy for cancer chemotherapy has showed preferential ability to deliver antitumor therapeutics precisely to tumor sites by enhanced permeability and retention (EPR) effect, which mainly due to the leaky nature of the tumor vasculature.[3] whereas there are several critical challenges remain unclarified such as random leakage of drugs and serious side-effects.[4-8] Therefore, the advance of highly integrated nanoplatforms for early diagnosis and effective therapy is urgently demanded. Because of the different physiological conditions between normal cells and tumor cells, nanoplatforms that are specifically responsive to the tumoral environmental cues and then activate their theranostic functionality are highly desirable. Since the commercial formulation of Doxil®[9], a myriad of amphiphilic polymers which are able to self-organize into supramolecular nanoarchitectures such as micelles, vesicles, fibers and nanoparticles etc. have been utilized as drug carriers to deliver chemotherapeutic agents due to the flexibility of structure engineering, high drug delivery efficiency and excellent biocompatibility.[10-17] However, the severe side-effects to normal cells and tissues remain a serious issue, which is mainly attributed to the undesired and nonspecific release of drugs.

In recent years, polymeric drugs are mainly limited to linear or nonlinear polymers. Aiming at specific tumor microenvironment, pH-responsive hydrazone linkers or redox-sensitive disulfide linkages had been broadly studied as a strategy to inhibit unspecific drug release in physiological environment.[18-20] Among various existing polymeric nanoplatforms, unimolecular micelles (UMs) based on single macromolecules of star-like,[21-28] cycle-like,[29-31] brush-like

or hyperbranched polymers[32-34] are featured by controlled size and robust micellar stability, representing an straightforward method to address the aforementioned general issues of nanomedicine. As a polysaccharide polymer, β-cyclodextrin (β-CD) possessed 21 hydroxyl groups and was an ideal initiator for well-defined star-like polymers.[35] Previously, we reported one type of robust UMs based on a star-like block copolymer of β-cyclodextrin (β-CD) grafting poly(lactic acid)-*b*-poly(ethylene glycol) shell, which could effectively improve the stability of polymeric micelles and restrain early release of drugs.[36-37] However, there was a major limitation that the drugs were loaded into the micelles through a physical absorption between drugs and carrier rather than a cleavable covalent bond.[38] Recently, Jia and co-workers designed a well-defined star-like block copolymer-doxorubicin conjugates through hydrazone-based linkage, which exhibited effective therapeutics against cancer cells.[21] Furthermore, Qiu and co-workers utilized hyperbranched hydrophilic UMs for delivery of anticancer drug camptothecin (CPT) *via* acid-labile β-thiopropionate linkage, which showed pH-triggered CPT release behavior.[39] In spite of their attracting new features, these micellar systems are still not able to systematically address the major issues such as restricted drug loading rate, undesired side-effect to normal tissues and insufficient efficacy for theranostics purpose.

Herein, we report an acid-responsive amphiphilic star-like prodrug that integrates the diagnostic and therapeutic functionality into one on-demand system. The obtained UMs consist of a diblock copolymer poly(2-methoxy-2-oxoethyl methacrylate modified doxorubicin)-*b*-poly[(ethylene glycol) methyl ether methacrylate] extended from the β-cyclodextrin (β-CD) core (β-CD-P(DOX)-*b*-P(OEGMA), abbreviated as DOX@CPMO) (Scheme 1). Compared to previously reported methods about unimolecular micelles derived from amphiphilic

diblock copolymers, the present design of star-like prodrug has well-defined chemical structures, high drug loading rate, high micellar stability and stimuli-responsive drug release capability, which may produce an enhanced therapeutic effect on tumor cells or tissues. Specifically, the ratio of hydrophobic PDOX chain and hydrophilic chains POEGMA could be adjusted resulting in tailorable micellar size and drug loading rate. The DOX@CPMO had a maximum drug loading rate of 53.1 wt % and was responsive to the acidic tumor microenvironment with enhanced fluorescence intensity and simultaneously triggered drug release. More importantly, DOX@CPMO micelles exhibited exceptional inhibition effect on HeLa and MCF-7 tumor cells, while minimal cytotoxicity against normal HUVEC cells was observed. Further investigations *in vitro* on cellular internalization and uptake efficiency of the drugs demonstrated that the micelles could realize selective drug accumulation in tumor cells, showing the potential as a promising nanoplatform for cancer therapy.

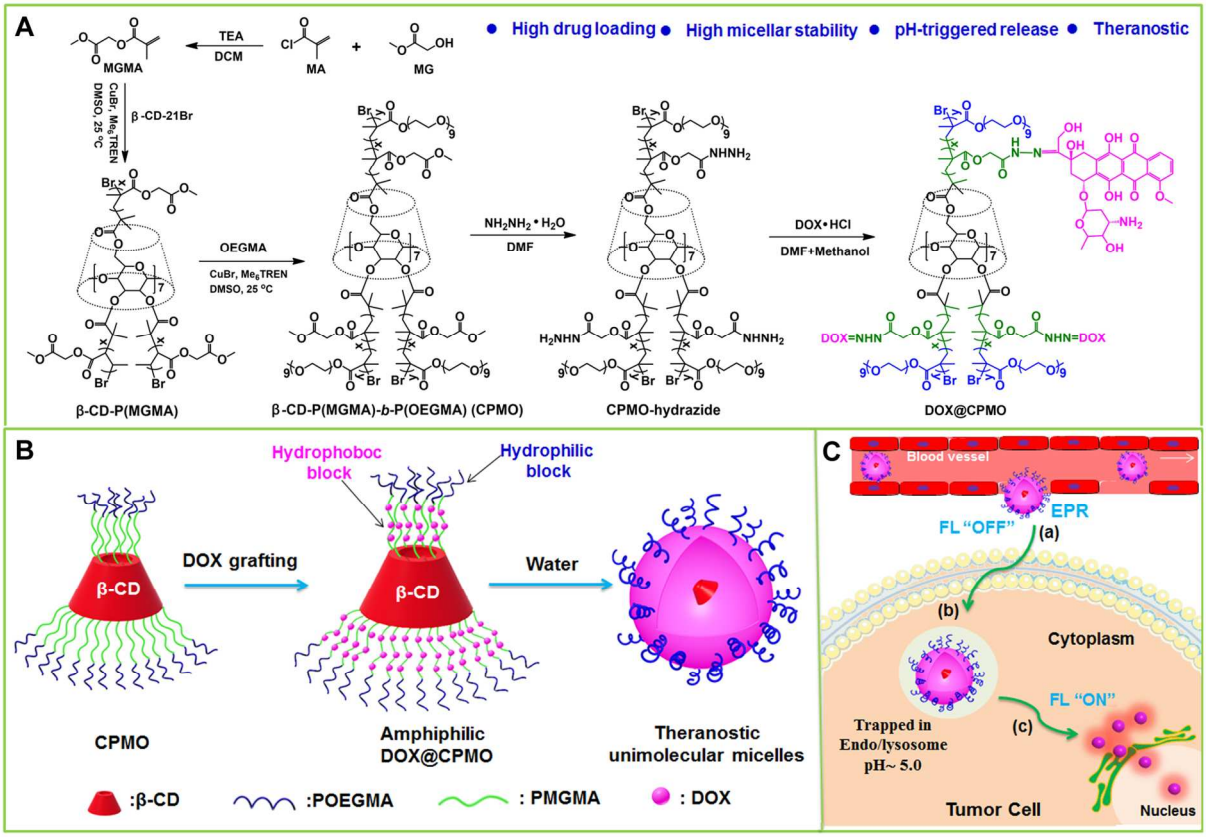

Scheme 1. (A) The synthetic route of DOX@CPMO polymeric prodrug. (B) Schematic diagram of DOX@CPMO as a theranostic platform for cancer therapy. (C) The enhanced permeability and retention (EPR) effect-mediated cell endocytosis and fluorescence (FL) ON-OFF process: (a) The DOX@CPMO UMs entering a tumor cell mediated by EPR effect (FL-OFF); (b) DOX@CPMO UMs were trapped in endo/lysosomes; (c) DOX was delivered into nucleus by pH-triggered release (FL-ON), realizing theranostic functionality of UMs.

EXPERIMENTAL SECTION

Materials. All chemical reagents including methyl glycolate, methacryloyl chloride, β-cyclodextrin (β-CD, 99.7 %), Poly(ethylene glycol) methyl ether methacrylate (OEGMA), triethylamine (TEA, 99 %), Hydrazine hydrate, copper(I) bromide (CuBr, 98.0 %), Tris(2-

dimethylaminoethyl)amine (Me_6TREN) were purchased from Sigma-Aldrich (USA). After washing thrice with acetic acid and acetone, respectively, copper(I) bromide was dried and placed in a glove box. The inhibitors in OEGMA were removed using an alumina column before using. Dichloromethane (DCM) and trifluoroacetic acid (TFA) were obtained from Aladdin. Doxorubicin hydrochloride (DOX·HCl) was supplied by Beijing HuaFeng United Technology Co. Ltd (China). All anhydrous solvents including anhydrous N, N-Dimethylformamide (DMF), Dimethylsulfoxide (DMSO) and anhydrous methanol were supplied by Sigma-Aldrich (USA). All reagents were used directly unless otherwise noted.

Characterization. ^{1}H NMR spectra were obtained using Bruker AV 600 NMR spectrometer (Rheinstetten, Germany) employing tetramethylsilane (TMS) as an internal reference at 25 °C. The size distribution of the obtained micelles were detected by dynamic light scattering (DLS) on a Nano ZS90 (Malvern, UK) with angle detection at 90 °C. The micellar morphology was detected trough a JEM-1230EX transmission electron microscopy (TEM) (Japan). Micelle samples for TEM detection were obtained using the following method: one droplet of the micelle samples in water was cast on carbon-coated copper grids held by tweezers and dried in air at room temperature. Fourier transform infrared (FTIR) spectra were acquired on a Thermo Nicolet 6700 FTIR spectrophotometer (USA) and KBr pellets were used as tablet. The number-average molecular weight (Mw) and distribution (Mw/Mn) were measured using a gel permeation chromatography (GPC) system (Agilent 1260, USA) equipped with Agilent 1260 pump and a Agilent 1260 refractive index detector and a styragel$^{®}$HT column. Tetrahydrofuran (THF) was used as the eluent (1 mL/min), and polystyrene was used as the standard for calibration. Fluorescence spectrum was measured on a Shimadzu RF-5301PC fluorescence spectrometer (Shimadzu, Japan). Absorbance spectrum was obtained using a Shimadzu UV-1800 visible

spectrophotometer (Shimadzu, Japan). Fluorescence images were recorded using a confocal laser scanning microscope (CLSM 800, Carl Zeiss, Germany). Cellular uptake efficiency of drugs was measured by flow cytometry (NovoCyte 2060R, USA).

Synthesis of 2-methoxy-2-oxoethyl methacrylate (MGMA) monomer. Firstly, MGMA monomer was synthesized following a previous report with some modification.[39] Methyl glycolate (6.48 g, 0.072 mol) and TEA (20 mL, 0.144 mol) were dissolved in dry dichloromethane (DCM, 50 mL) under 0 °C ice bath. Then Methacryloyl chloride (7.251 mL, 0.072 mol) in 30 mL DCM was added dropwise using a syringe pump followed by 2 h stirring at 0 °C. After continuous stirring for 20 h at room temperature, the obtained mixture was filtered to remove the by-product of triethylamine hydrochloride precipitate. Subsequently, the solvent was concentrated by evaporation, and the crude product was purified by column chromatography with an ethyl acetate/hexane mixture (1/2, v/v, R_f = 0.2-0.3 on silica). The product was isolated by evaporation and further dried in a vacuum oven, yielding a colorless oily residue. (9.55 g, 78 % yields). ^{1}H NMR (600 MHz, $CDCl_3$): δ 1.93 (s, 3H), 3.72 (m, 3H), 4.64 (s, 2H), 5.62 (s, 1H), 6.17 (s, 1H).

Synthesis of star-like β-CD-PMGMA block. The β-CD-PMGMA block polymer was synthesized based on conventional ATRP reaction using β-CD-21Br as the initiator.[41] Typically, β-CD-21Br (22.5 mg, 0.005 mmol), MGMA (680 mg, 4.2 mmol) and CuBr (15.2 mg, 0.105 mmol) were dissolved in 3 mL anhydrous DMSO in a 10 mL two-neck flask under argon atmosphere. After three degassing cycles using liquid nitrogen, the ligand of Me_6TREN (46 uL, 0.21 mmol) was added into the above mixture. The reaction was carried out at 25 °C with continuous stirring for 12 h and was stopped by liquid nitrogen. The THF diluted mixture was passed through a neutral Al_2O_3 column, concentrated and precipitated into excess diethyl ether.

The acquired precipitate denoted as β-CD-PMGMA was dried at room temperature under vacuum, yielding a sticky liquid (225.6 mg, 33.1 % yields).

Synthesis of star-like β-CD-PMGMA-POEGMA (CPMO) diblock copolymer. The diblock copolymer of β-CD-PMGMA-POEGMA was synthesized by an ATRP reaction using the β-CD-P MGMA as a macroinitiator reacted with OEGMA. Briefly, β-CD-PMGMA (128 mg, 0.001 mmol), OEGMA (287 mg, 0.525 mmol) and CuBr (3.1 mg, 0.021 mmol) were dissolved in a mixture solvent of 2.0 mL anhydrous DMF and 2.0 mL anhydrous DMSO in a 25 mL two-neck flask under argon atmosphere. After three repeated degassing procedures, Me_6TREN (7.5 uL, 0.021 mmol) was injected into above mixture and subjected to two cycles of freeze-pump-thaw. The polymerization was carried out at 25 °C with constant stirring for 20 h. The reaction was terminated by putting the solution into liquid nitrogen and removing the catalyst using a neutral Al_2O_3 column, concentrated and then precipitated into excess diethyl ether. The obtained precipitate was dried at room temperature under vacuum, yielding a sticky liquid (150.2 mg, 36.2 % yields).

Synthesis of star-like CPMO-hydrazide diblock copolymer. Typically, CPMO diblock copolymer (100 mg) and hydrazine hydrate (0.75 ml) were dispersed in a mixed solvent of 5 mL methanol and 2 mL DMF in a 25 mL flask under protection of argon atmosphere. The reaction was carried out at room temperature with continuous stirring for 10 h. Then, the mixture was dialyzed (MW 3500) against DI water (500 mL ×3) for 2 days. Finally, the solution was freeze-dried to obtain a pale solid, denoted as CPMO-hydrazide.

Synthesis of star-like DOX@CPMO prodrug. Typically, CPMO-hydrazide (100 mg, 0.064 mmol) and DOX·HCl (100 mg, 0.16 mmol) were dissolved into a mixture solvent of 3 mL

anhydrous DMF and 3 mL anhydrous methanol in a 25 mL flask, and one drop of TFA was added under argon atmosphere. Then, the mixture was stirred under dark for 48 h at room temperature. To thoroughly remove the unreacted DOX molecules， the mixture was dialyzed (MW 3500) against methanol (200 mL ×3) for 2 days. Finally, the dialysis solution was freeze-dried yielding a reddish brown solid.

Preparation of DOX@CPMO unimolecular micelles (UMs) in different solvent. Typically, 10 mg DOX@CPMO prodrug was directly dissolved in 10 mL DMF with continuous stirring for 6 h and DOX@CPMO UMs in DMF was obtained with a concentration of 1.0 mg/mL.

Next, DOX@CPMO UMs in water was acquired *via* a dialysis method. 5.0 mg DOX@CPMO prodrug was firstly dissolved in 1.0 mL DMF with continuous stirring for 1 h, and the solution was added dropwise into 6 mL deionized water with continuous stirring for another 1 h. The resulting solution was dialyzed using dialysis bag (MW 3500) against deionized water (1000 mL ×3) for 48 h and the concentration of UMs was adjusted to 500 μg/mL.

***In vitro* DOX drug release.** The *in vitro* release of DOX drug from DOX@CPMO UMs was carried out by a dialysis method. Firstly, 1.0 mL of the micellar solution was transferred into a dialysis bag (MW 3500) and immersed into 80 mL of fresh phosphate buffered saline (PBS) solution with different pH value (pH = 5.0, 6.8 or 7.4) at 37 ± 1 °C with slight shaking, respectively. 1.0 mL external solution was collected and 1.0 mL fresh buffer was added at designated time points. The concentration of DOX was calculated based on the calibration curve of DOX by fluorescence spectroscopy under excitation at 488 nm and emission at 550 nm. All release experiments were measured in triplicate.

Cytotoxicity. Cell viability of DOX@CPMO UMs were estimated via PrestoBlue assays against HeLa, MCF-7 and HUVEC cells lines. Firstly, HeLa, MCF-7 and HUVEC cells were cultured in Dulbecco's Modified Eagle's Medium (DMEM) containing 10 % fetal bovine serum (FBS) and 1 % penicillin/streptomycin (P/S) with 5 % CO_2 at 37 °C. Then cells were incubated in 96-well plates with a density of 1×10^4 cells per well for 12 h at 37 °C with 5 % CO_2. The medium was washed with PBS (1×) and replaced with fresh DMEM containing different concentrations of free DOX or DOX@CPMO. After 72 h incubation, the culture solution was discarded and PrestoBlue reagent diluted with DMEM medium was added to each well and incubated at 37 °C with 5 % CO_2. After 1 h incubation, the absorbance at 570 nm (reference wavelength is 600 nm) was measured using a plate reader (Tecan Infinite spark10 series Pro, Tecan Asia, Singapore). All samples were tested in triplicate. Cells without treatment served as control and the corresponding cytotoxicity was set as 100 %. Then, the obtained data were analyzed following the provided protocol. Meanwhile, the cytotoxicity of blank CPMO UMs was investigated based on HeLa cells and MCF-7 cells using similar method.

Fluorescence images. Fluorescence images of HeLa and MCF-7 cells treated with DOX@CPMO UMs were recorded using confocal laser scanning microscopy (CLSM). HeLa and MCF-7 cells were incubated in 6-well plates with a density of 1×10^4 cells per well for 12 h at 37 °C with 5 % CO_2. Then, the medium was replaced with fresh DMEM containing free DOX and DOX@CPMO (equivalent DOX concentration 20 ug/mL) and further cultured for 0.5, 2 and 6 h, respectively. After that, the culture solution in each well was removed and the cells were washed for five times with PBS (1×). Then the cells were treated with formalin solution for 30 min and then washed with PBS (1×) for three times. After that, the cells were permeabilized with 0.1 % (vol/vol) Triton X-100 for 5 min and blocked with 1 % (wt/vol) BSA for 30 min. After

washing twice with PBS, the cells were stained with Alexa Fluor 633 phalloidin for 1 h and DAPI for 1 min. Finally, the cells were washed and resuspended in fresh PBS for imaging. For fluorescence microscopy, DAPI, DOX, and Alexa Fluor 633 phalloidin were excited under 405, 488, and 633 nm, respectively. The corresponding fluorescent emissions were recorded by a confocal laser scanning microscope (CLSM 800, Carl Zeiss, Germany) using a band-pass filter combination including 410-507 nm, 493-634 nm, and 638-747 nm (Objective: EC Plan-Neofluar 20x/0.30 M27).

***In vitro* lysosome colocalization by CLSM.** The localization of DOX@CPMO micelles in HeLa cells were analyzed to trace their path into cells. Firstly, HeLa cells were incubated in a 6-well plate and cultivated for 12 h with 5 % CO_2 at 37 °C. Then, DOX@CPMO-1 or DOX@CPMO-2 (final DOX concentration: 20 μg/mL) were introduced into the culture medium. After 0.5 h, 2 h or 6 h incubation, the cell culture medium was removed and each well was washed with PBS (1×) for five times. After that, the cells were stained with Lyso Tracker@Red dye diluted with DMEM for 0.5~1 h. Finally, the cells were washed with PBS (1×) before imaging.

Cellular uptake. *In vitro* cellular uptake experiments were evaluated with HeLa cells by flow cytometry. HeLa cells were incubated in 6-well plates with a density of 1×10^4 cells per well for 12 h at 37 °C with 5 % CO_2. Then, the medium was replaced with fresh DMEM containing DOX@CPMO-1 or DOX@CPMO-2 UMs (DOX concentration: 20 ug/mL) and the cells were cultured further for 2, 4, 6 or 12 h, respectively. Afterwards, every well was washed with PBS (1×) thrice to remove excess drugs. Then the cells were trypsinized with TrypLE Express. After centrifugation, the supernatant was discarded and the cells were resuspended in PBS (1×) (500 μL) for flow cytometry. The fluorescence intensity of DOX@CPMO UMs were recorded under excitation of 488 nm and emission of 500-560 nm based on approximately 1×10^4 gated cells. The

untreated cells were used as control. The flow cytometry data were analyzed using FlowJo software.

RESULTS AND DISCUSSION

Synthesis of the star-like DOX@CPMO prodrug

The synthetic route of star-like DOX@CPMO prodrug is shown in Scheme 1A. Firstly, a macroinititor, denoted as β-CD-21Br, was synthesized *via* the reaction of β-CD and 2-bromoisobutyryl bromide (BIBB) following a previous report (Figure S1). Then the star-like β-CD-PMGMA polymers with adjustable block length were synthesized *via* ATRP reaction of 2-methoxy-2-oxoethyl methacrylate (MGMA) by adding CuBr catalyst and Tris(2-dimethylaminoethyl)amine (Me_6TREN) ligand at 25 ^{o}C, resulting in two block polymers of β-CD-P$(MGMA)_{18}$ and β-CD-P$(MGMA)_{30}$. Next, the hydrophilic poly(ethylene glycol) methyl ether methacrylate (OEGMA) monomer was grafted at the end of β-CD-PMGMA block *via* ATRP reaction, resulting in two star-like diblock copolymer of β-CD-P$(MGMA)_{18}$-*b*-P$(OEGMA)_5$ (CPMO-1) and β-CD-P$(MGMA)_{30}$-b-P$(OEGMA)_9$ (CPMO-2). Finally, the DOX@CPMO prodrugs were subjected to reaction with hydrazine hydrate and immediate conjugation with DOX·HCl drug. The structural parameters of β-CD-PMGMA-POEGMA star-like polymers was summarized in Table 1.

Table 1. Structural characterization of the star-like polymers of β-CD-PMGMA-POEGMA.

Polymer [a]	$M_{n,NMR}$ [b] (g mol^{-1})	$M_{n,GPC}$ [c] (g mol^{-1})	M_w/M_n [d]	D [e] (Water)	D [e] (DMF)	LC [f] (wt%)
β-CD-P(MGMA)$_{18}$	65700	12700	1.39	—	—	—
β-CD-P(MGMA)$_{30}$	106500	32000	1.36	—	—	—
β-CD-P(MGMA)$_{18}$-*b*-P(OEGMA)$_5$	118200	41000	1.38	25.28	28.85	53.1±2.6
β-CD-P(MGMA)$_{30}$-b-P(OEGMA)$_9$	201000	51900	1.37	34.87	39.36	46.1±1.8

[a] DP_{MGMA} and DP_{OEGMA} are the degree of polymerization of MGMA and OEGMA, calculated from ^{1}H NMR data. [b]Number-average molecular weight, $M_{n,NMR}$ calculated from ^{1}H NMR data.[c] Number-average molecular weight, $M_{n,NMR}$ determined by GPC. [d] Polydispersity index, PDI determined by GPC. [e]Hydrodynamic diameter of prodrug micelles in different solvent were measured by DLS. [f]The loading content (LC) were determined by fluorescence (FL) spectrophotometer, and the data are presented as means ± SD (n = 3).

The ^{1}H NMR results of MGMA monomer and β-CD-P(MGMA)$_{18}$ block were presented in Figure S2 and Figure S3, respectively. The characteristic peaks of MGMA appeared at 6.17 and 5.62 ppm (Peak a and b corresponding to alkene protons), 4.65 ppm (Peak d, methylene protons close to ester group), 3.72 ppm (Peak e, methoxy group), and 1.94 ppm (Peak c, methyl group close to carbon-carbon double bond). Additionally, the representative signals of MGMA at 4.59 and 3.76 ppm were recorded in the ^{1}H NMR results of β-CD-P(MGMA)$_{18}$ block, indicating the successful polymerization of MGMA. The ^{1}H NMR results of β-CD-P(MGMA)$_{18}$-*b*-P(OEGMA)$_5$ (CPMO-1), CPMO-1 hydrazide, free DOX and DOX@CPMO-1 are shown in Figure 1. The signals at 3.65 ppm (Peak 3, methylene protons close to methoxy group) and 3.38 ppm (Peak 4, the methoxy group on the terminal of POEGMA) of OEGMA indicated that CPMO-1 was synthesized successfully. Furthermore, the representative peak of MGMA at 3.72 ppm disappeared in the ^{1}H NMR results of CPMO-1 hydrazide, suggesting that methoxy group of MGMA was replaced by hydrazine group totally. After grafting with DOX, the characteristic peaks 1 and 2 of DOX were observed in the ^{1}H NMR spectra of DOX@CPMO-1 prodrug. To

study the structural effect on the drug loading rate and the hydrophilicity of the prodrug, we synthesized two amphiphillic prodrugs by altering the ratio of hydrophilic and hydrophobic blocks. We found that the drug loading rate of DOX@CPMO-1 and DOX@CPMO-2 could reach 53.1±2.6 wt % and 46.1±1.8 wt %, respectively. These were substantially higher than our previously developed star-like β-CD-PLA-POEGMA drug delivery system,[36] in which the drug loading mainly depended on the hydrophobic-hydrophobic interaction of PLA or PDPA chain and DOX drug. More importantly, the covalent hydrazone bond could considerably improve the micellar stability of DOX@CPMO micelles and realize controlled drug release.[42-43]

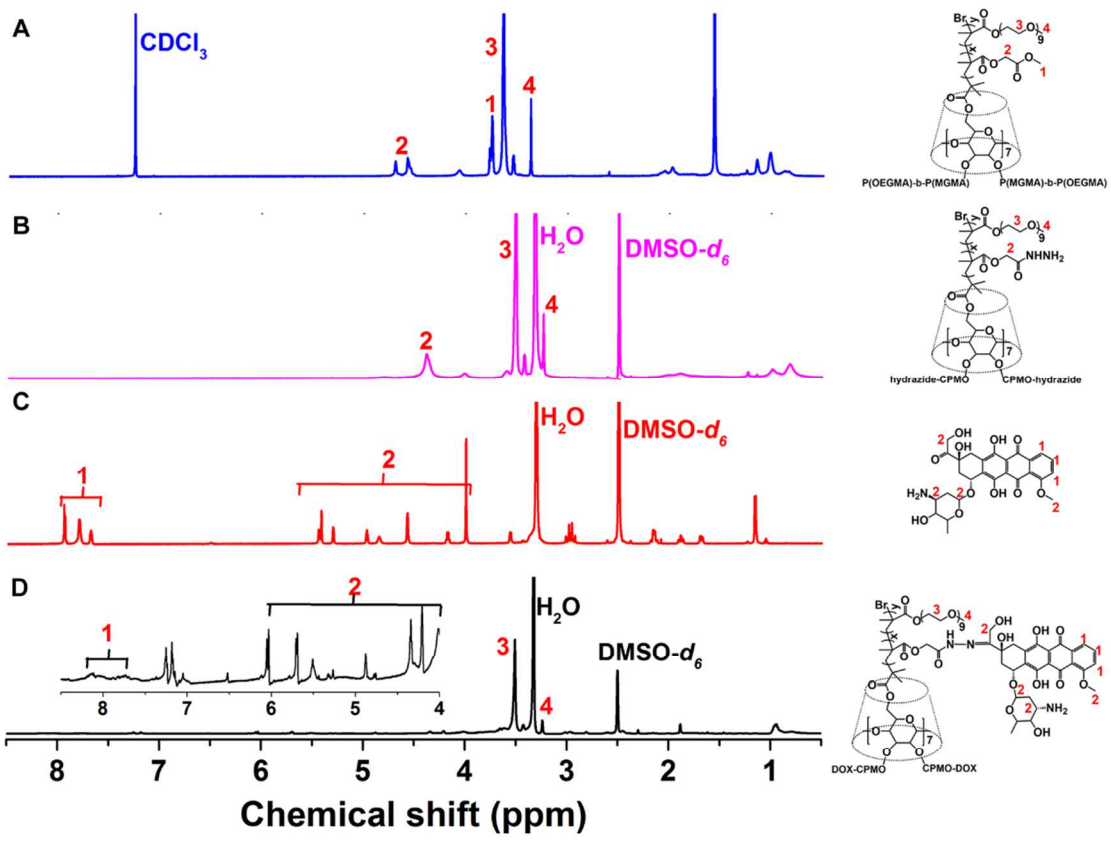

Figure 1. ^{1}H NMR spectra in $CDCl_3$ or DMSO-d_6 of (A) β-CD-P(MGMA)$_{18}$-*b*-P(OEGMA)$_5$ (CPMO-1) , (B) CPMO-1 hydrazide, (C) free DOX and (D) DOX@CPMO-1 prodrug.

Gel permeation chromatography (GPC) technology was used to trace the polymeric process of CPMO diblock copolymer. As shown in Figure 2 and Table 1, two CPMO and their precursor polymers all exhibited a monomodal peak, and their polydispersity indices (PDI) were all less than 1.4, suggesting the successful synthesis of CPMO diblock copolymer. As summarized in Table 1, two star-like copolymers of β-CD-P(MGMA)$_{18}$-*b*-P(OEGMA)$_5$ and β-CD-P(MGMA)$_{30}$-*b*-P(OEGMA)$_9$ were prepared. FTIR analysis was used to obtain further evidence of the synthesized DOX@CPMO polymer (Figure S4). Specifically, the –COO– stretching peak of MGMA appeared at 1759 cm^{-1} and 1735 cm^{-1}, and the –O–CH$_3$ stretching vibration of OEGMA appeared at 1103 cm^{-1}, indicating the successful polymerization of CPMO. In addition, the new stretching peak at 1652 cm^{-1} corresponding to –C=N– in the hydrazone bond implied that DOX was loaded in the CPMO prodrug.

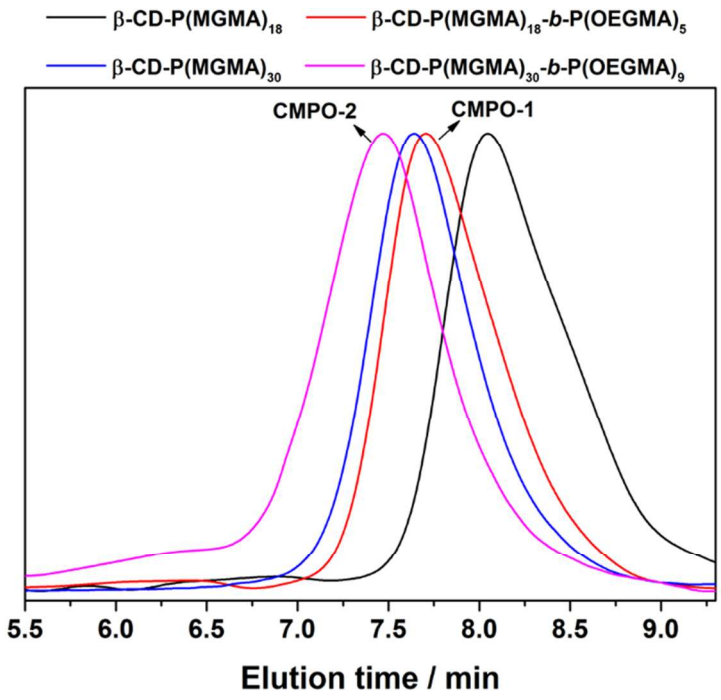

Figure 2. The GPC chromatograms of star-like CPMO diblock copolymer and their previous product in THF.

Size and morphology of DOX@CPMO UMs

Due to the well-defined structure, these amphiphilic DOX@CPMO prodrugs were able to form UMs in water solution. We used transmission electron microscopy (TEM) to track the morphology of the UMs. As shown in Figure 3A and D, the DOX@CPMO UMs exhibited nearly spherical morphology, which was attributed to the star-like nanostructure of DOX@CPMO. The dehydrated form of UMs under TEM showed average diameters of 17.8 ± 3.7 nm and 23.2 ± 2.8 nm for DOX@CPMO-1 and DOX@CPMO-2, respectively. The larger size of latter could be due to its higher molecular weight.

The dynamic light scattering (DLS) method was employed to characterize the UMs dispersed in water solution and an organic solvent. Figure 3B and E demonstrated that the average diameters of these two UMs were approximately 25.28 nm and 34.87 nm, respectively. Compared to the sizes obtained using TEM, the larger micellar sizes as measured by DLS were mainly due to the hydration of the POEGMA shell in aqueous solutions, [44] which was a common phenomenon also found in other types of UMs such as the β-CD-PLA-POEGMA UMs reported previously.[36] Additionally, the UMs showed further size increase in DMF, an organic solvent that had a good solubility for the hydrophobic core of DOX and the hydrophilic chain of POEGMA. The micellar sizes of these two UMs in DMF (Figure 3C and F) were approximately 28.85 nm and 39.36 nm, respectively, which were greater than their corresponding sizes in water and suggested that the DOX@CPMO prodrug could fully dissolved in DMF solution without intermolecular aggregation. On the other hand, these results also implied the successful formation of UMs in water solution.[37]

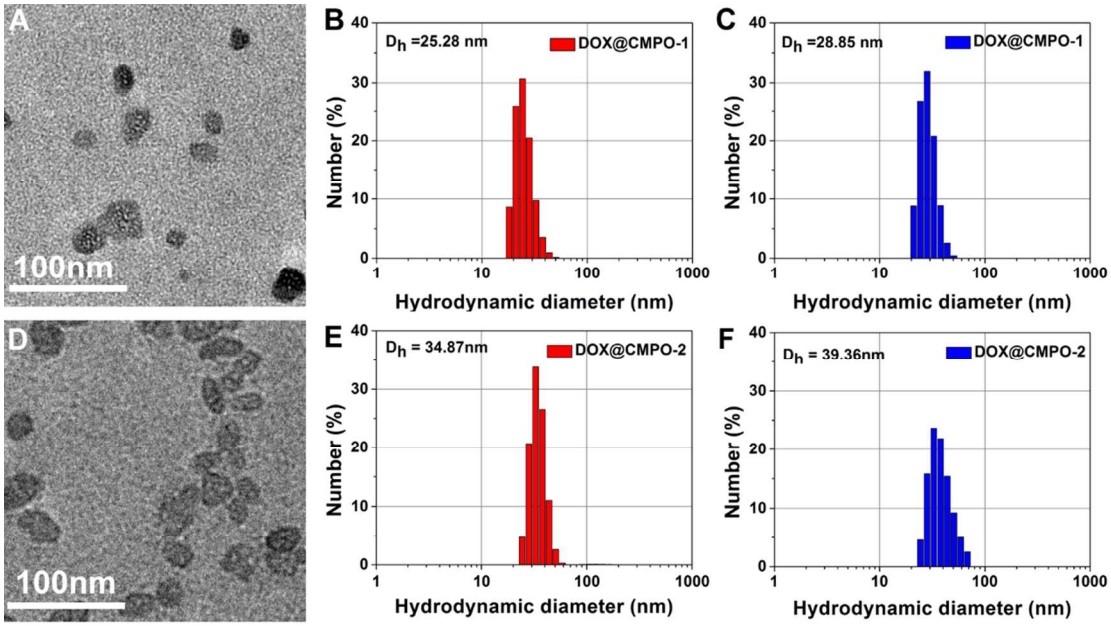

Figure 3. TEM images of DOX@CPMO-1 (A) and DOX@CPMO-2 (D) UMs; The DLS histograms of DOX@CPMO-1 and DOX@CPMO-2 UMs in water (B and E) and DMF solvent (C and F).

The UV-vis absorption and fluorescence intensity of DOX@CPMO UMs in water and DMF were measured to study their drug loading capability. In Figure S5, both of these DOX@CPMO micelles in DMF or water showed strong absorption approximately at 488 nm, which was characteristic absorption of the grafted DOX. Furthermore, the maximum fluorescence intensity of DOX@CPMO micelles was at about 585 nm in aqueous or DMF media (Figure S6). Compared to free DOX, the red shift of DOX@CPMO micelles in water could be attributed to the intermolecular aggregation of DOX in the micelles. The larger red shift of DOX@CPMO micelles in DMF than that in aqueous solution could be due to the higher polarity of DMF.[21]

We further examined the fluorescence intensity of DOX@CPMO UMs in different pH conditions and solvents (DOX concentration: 10.0 ug/mL). As shown in Figure 4 A and B, the DOX@CPMO UM solutions in PBS solution or DMF were reddish under ambient light.

Interestingly, intensive fluorescence of DOX@CPMO UMs was observed under pH = 5.0 after 24 h of incubation and in DMF solution with UV irradiation, while there was weak fluorescence under pH = 7.4. We speculated that the fluorescence of DOX was suppressed in the hydrophobic core of UMs under pH = 7.4 due to the poor solubility of DOX in neutral aqueous solutions, and the pH-responsive hydrazone bond further maintained the stability of the UMs. The pH-dependent fluorescence was quantitatively confirmed by fluorescence emission spectra of above DOX@CPMO UMs solutions (Figure 4C). Interestingly, when the aqueous solution became acidic (pH = 5.0), the fluorescence intensity recovered strongly attributed to the breakage of hydrazone bond and the escaped DOX from the UMs. The fluorescence intensity at around 585 nm in pH 5.0 was approximately 20-fold and 7-fold than that in pH=7.4 for DOX@CPMO-1 and DOX@CPMO-2 (Figure S7), respectively. Moreover, the fluorescence intensity of DOX also recovered slightly when the UMs were exposed to DMF, which is a good solvent for both DOX and POEGMA. These results demonstrated the potential of the DOX@CPMO prodrug as a fluorescent probe activated by the acidic microenvironment.[45-46]

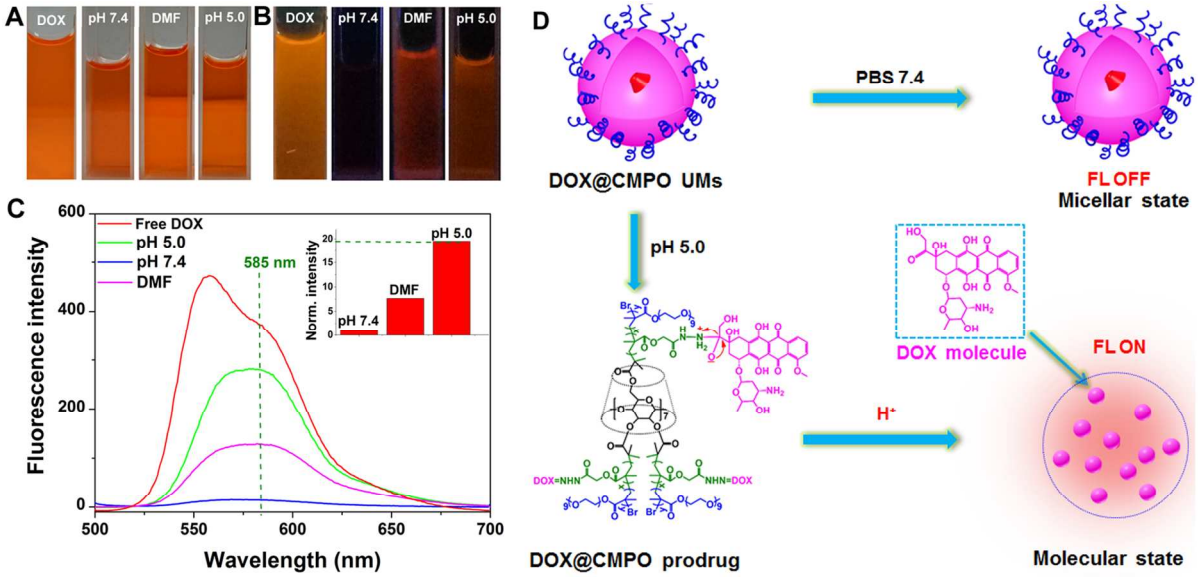

Figure 4. The images of free DOX and different DOX@CPMO-1 solutions under (A) visible light and (B) UV irradiation (365 nm); (C) The fluorescence emission spectra of different DOX@CPMO-1micelles (λ_{exc} = 488 nm) and the inset histogram shows the normalized fluorescence intensity of different DOX@CPMO-1 solutions; (D) The proposed mechanism leading to the pH-triggered DOX release and pH-depending enhanced fluorescence intensity.

***In vitro* release and cytotoxicity**

The anticancer drug of DOX was grafted on the core of the star-like CPMO diblock copolymer by covalent hydrazone bond, which could enable controlled drug release in response to acidic environment. Due to the longer PMGMA block of CPMO-2 than that of CPMO-1, the drug loading rate was 53.1 wt % in DOX@CPMO-2 while 46.1 wt % in DOX@CPMO-1. The loading rate were calculated according to the fluorescence standard curve of DOX in water solution. The *in vitro* drug release profiles of DOX@CPMO UMs were obtained under different solutions (pH = 7.4, 6.8 or 5.0) at 37 °C under gentle vibration. As shown in Figure 5A-B, the drug release of DOX@CPMO under simulative tumor microenvironment (pH = 5.0) was faster than that under neutral physiological environment (pH = 6.8 or 7.4). The cumulative drug release of DOX@CPMO in 96 h reached nearly 80 % under pH = 5.0, while only about 10 % under pH = 6.8 or 7.4. DOX@CPMO-2 released slightly higher amount of drug than DOX@CPMO-1, which could be due to its higher drug loading rate as mentioned above. These results demonstrated the effective response of the DOX@CPMO prodrug to the tumor-specific acidic environment, which could minimize the toxicity to normal cells or tissues.

The cytotoxicity of the prodrug micelles was evaluated using PrestoBlue assay based on two tumour cell lines including HeLa and MCF-7 and a normal cell line of HUVECs. As shown

in Figure 5D-E, the DOX@CPMO-1 and DOX@CPMO-2 UMs (DOX concentration: 10 μg/mL) could dramatically reduce the viability of HeLa cells to 31% and 26% in 72 h, respectively. The cytotoxicity of these two UMs was even stronger against MCF-7 cells with approximately 1% and 12% final cell viability after 72 h, respectively. However, the drug-free CPMO-hydrazide micelles did not show obvious cytotoxicity on HeLa or MCF-7 cells, which maintained viability above 85% after 72 h treatment (Figure 5C) suggesting the excellent biocompatibility of the blank micellar carrier. In addition, we assessed the cytotoxicity of DOX@CPMO UMs against the HUVEC cells (Figure 5F). Obviously, free DOX destroyed the HUVECs unselectively under higher dosages, while treatment with DOX@CPMO UMs under the same DOX concentration could still maintain the cell viability above 65% after 72 h. These comparative studies indicated that delivery of antitumor DOX *via* CPMO micelles could effectively reduce the unspecific cytotoxicity of the pristine DOX to normal cells, whereas it can realize controlled drug release triggered by the tumor-specific environmental cues.[38, 47-48] Furthermore, the IC_{50} values of free DOX and star-like polymeric prodrugs was summarized in Table S1. This prodrug demonstrated the desirable features to minimize the side-effects while retain the maximal therapeutic effect for targeted diseases.

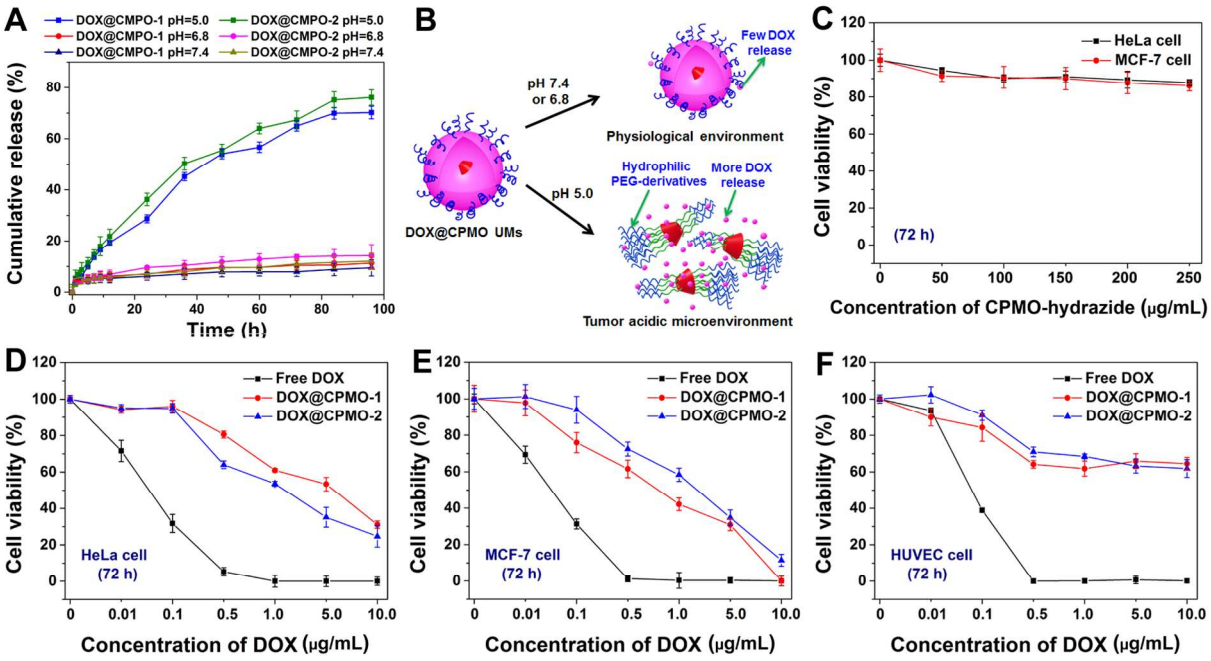

Figure 5. (A) DOX release from DOX@CPMO UMs in different PBS solutions (pH 7.4, 6.8 or 5.0) for 96 h at 37 ℃. (B) The schematic diagram of drug release in different pH conditions. (C) Viability of HeLa and MCF-7 cells cultured with CPMO-hydrazide blank micelles for 72 h. (D-F) The viability of HeLa cells (D), MCF-7 cells (E) and HUVEC cells (F) incubated with free DOX, DOX@CPMO-1and DOX@CPMO-2 under various DOX concentrations for 72 h. All the data are presented as means ± SD (n = 3).

Cell internalization of the prodrug

We used confocal laser scanning microscopy (CLSM) to investigate the cell internalization of the DOX@CPMO micelles in tumour cells. Herein, the CLSM images displayed the fluorescence of DOX (green), F-actin (Alexa Fluor 633 Phalloidin, red) and nuclei (DAPI, blue). The fluorescence intensity of internalized DOX mediated by CPMO micelles gradually increased with prolonged incubation time and accumulated mainly in the nuclei of HeLa cells after 6 h (Figure 6A or Figure S8). Similar phenomenon was also observed in MCF-7 cells (Figure S9 and

S10). In contrast, the intensive fluorescence of free DOX was observed rapidly within 2 h in the nuclei, which was mainly attributed to the diffusion of DOX molecules.

The cellular uptaking rate of DOX@CPMO micelles was analysed using flow cytometry. As shown in Figure 6B-C, Figure S11 and Figure S12, the uptaking rates of DOX@CPMO-1 and DOX@CPMO-2 gradually increased and reached 82.33% and 88.49% by 12 h, respectively, indicating the prominent internalization efficiency. The DOX@CPMO-2 exhibited slightly higher uptaking rate than DOX@CPMO-1, which was consistent to the higher drug release rate of the DOX@CPMO-2 (Figure 5A).

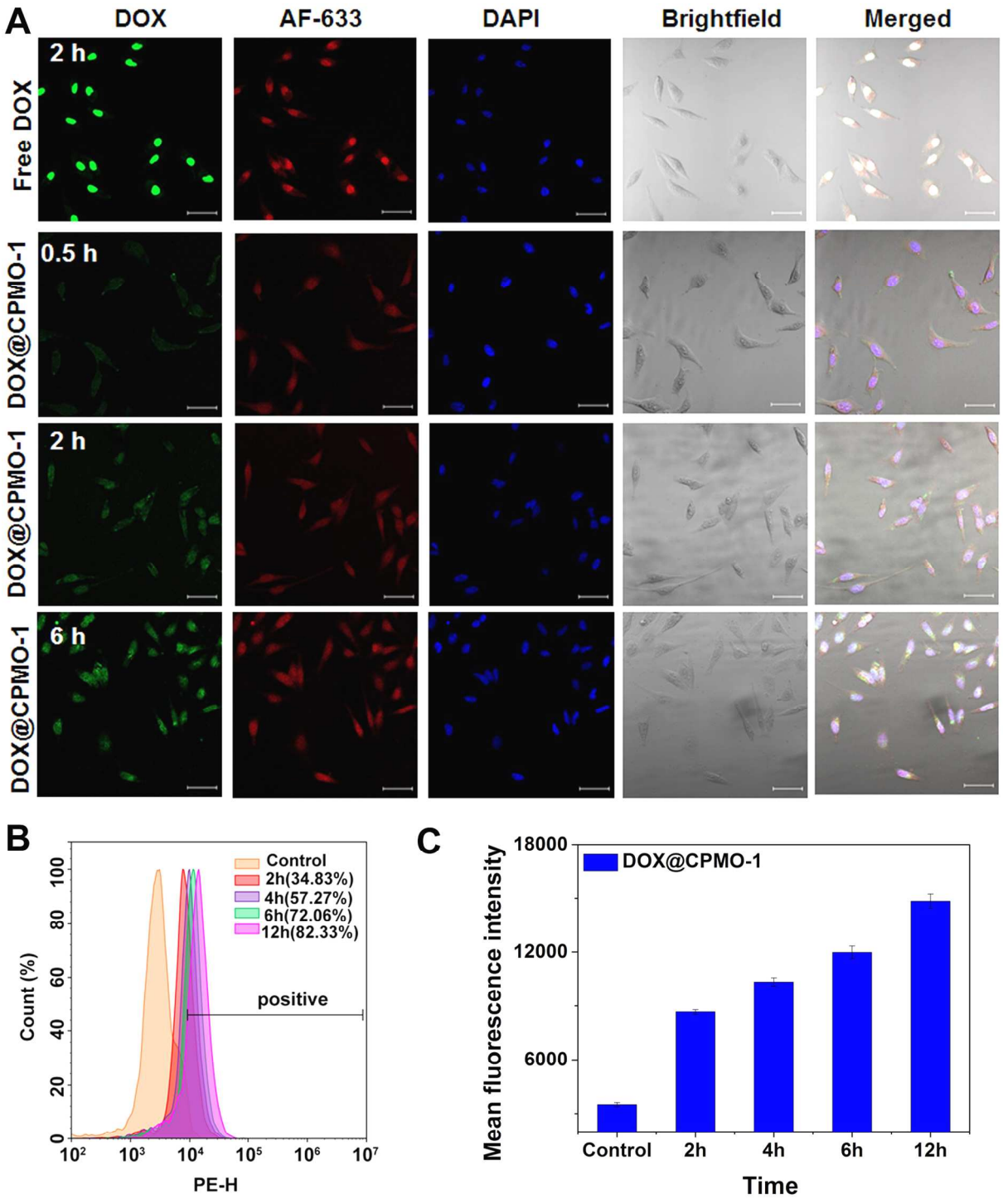

Figure 6. (A) CLSM and bright field images of HeLa cells incubated with free DOX or DOX@CPMO-1 micelles. (Equivalent DOX concentration: 20 μg/mL). The fluorescence of DOX, AF-633 and DAPI were pseudo-labeled as green, red and blue, respectively. Scale bars: 50 μm. (B) Flow cytometry analysis of the intracellular uptake of DOX@CPMO-1 micelles in HeLa

cells treated for 0, 2, 4, 6 and 12 h; (C) Mean fluorescence intensity of DOX@CPMO-1 micelles at different time points. The data were presented as the mean ± SD (n=3).

To further study the pathway of DOX@CPMO micelles into cells, Lyso Tracker@ Red was used to trace the co-localization of DOX@CPMO micelles in HeLa cells. As shown in Figure 7A and Figure S13, DOX@CPMO micelles firstly entered lysosomes. Initially, the DOX and Lyso Tracker@Red showed weak fluorescence, which was mainly located in the cytoplasm. After the incubation time increased to 6 h, the fluorescence of DOX extended to nuclei implying that DOX was released in response to the relatively lower pH condition in the lysosomes, while the Lyso Tracker@Red was still limited in cytoplasm. This co-localization experiment provided clear evidence for the endocytosis pathway during intracellular transport of the drug-laden micelles.[32, 49]

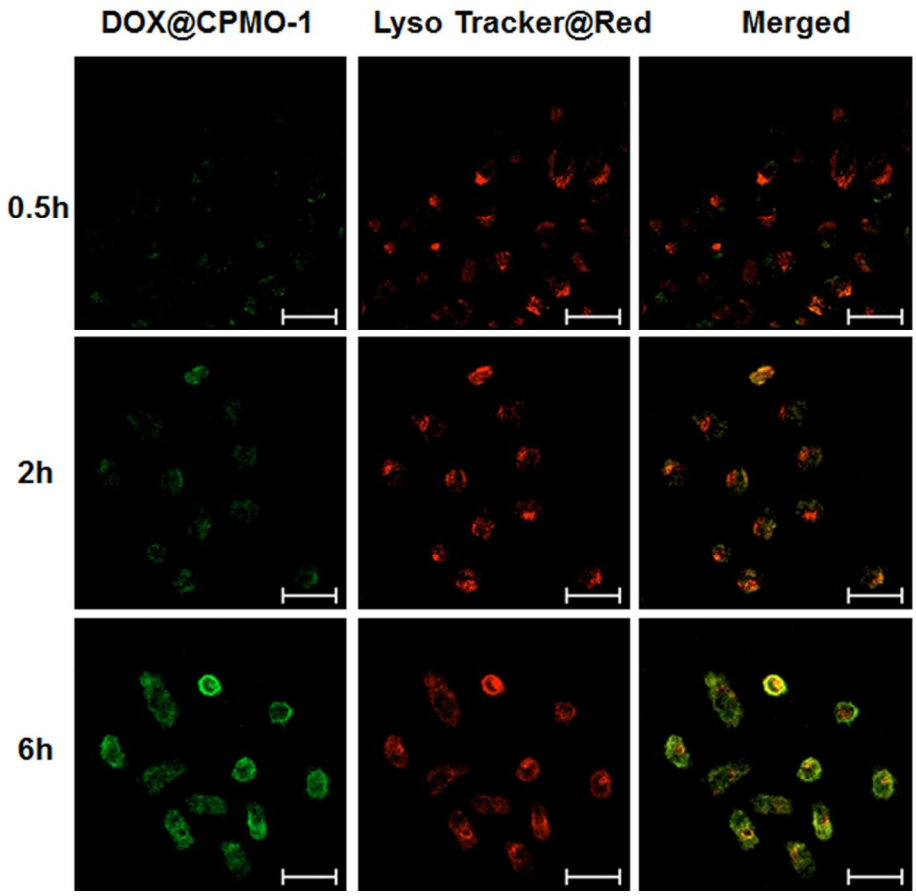

Figure 7. (A) CLSM images of HeLa cells after incubation with DOX@CPMO-1 micelles for 0.5, 2 and 6 h (equivalent DOX concentration: 20 μg/mL). The fluorescence of DOX, Lyso Tracker@Red was labeled as green and red, respectively. Scale bars: 50 μm.

CONCLUSIONS

In summary, we designed an acid-responsive amphiphilic star-like polymeric prodrug of DOX@CPMO, which integrates the features of high drug loading, high micellar stability, pH-dependent fluorescent diagnostics and pH-triggered drug release in one system. Specially, the amphiphilic DOX@CPMO prodrug could form stable UMs in water or DMF solution, and the size of DOX@CPMO UMs could be controlled by adjusting the ratio of hydrophobic PMGMA and hydrophilic POEGMA chains. The longer hydrophobic PMGMA chains were beneficial to the drug loading rate, which could be improved from 46.1 wt % to 53.1 wt %. Moreover, the DOX@CPMO UMs showed higher cytotoxicity against HeLa cells and MCF-7 cells but lower toxicity to normal HUVEC cells, suggesting a specific targeting capability on tumour cells. Furthermore, the DOX@CPMO UMs could act as a fluorescence nanoprobe to distinguish the tumour cells from normal tissues due to the pH-dependent fluorescence in response to the acidic tumour microenvironment. We believe that the present strategy could contribute to a promising nanoplatform for the clinical cancer diagnosis and therapeutics.

ASSOCIATED CONTENT

Supporting Information

^{1}H-NMR and FT-IR spectra; UV-vis absorption spectra and fluorescence spectra; CLSM images and Flow cytometry results. This material is available free of charge via the Internet at

http://pubs.acs.org.

AUTHOR INFORMATION

Corresponding Author

Z. Xu (zgxu@swu.edu.cn); Fax: +86-68253204; Tel: +86-68253792

Y. Kang (yjkang@swu.edu.cn); Fax: +86-68253204; Tel: +86-68254056

Funding Sources

This study was supported by a star-up grant (SWU115058, SWU115059), Fundamental Research Funds for Central Universities from Southwest University (XDJK2016A010) and the Basic and Frontier Research Project of Chongqing (cstc2016jcyjA0078) and National Natural Science Foundation of China (51703187, 31671037, 51503172).

Notes

The authors declare no competing financial interest.

REFERENCES

1. Ehrhardt, A. N. C.; Healy, A. M. Materials and methods for delivery of biological drugs. *Nat. Chem.* **2016**, *11*, 997-1007.
2. Tibbitt, M. W.; Dahlman, J. E.; Langer, R. Emerging frontiers in drug delivery. *J. Am. Chem. Soc.* **2016**, *3*, 704-717
3. Kobayashi, H.; Watanabe R.; Choyke, P. L. Improving conventional enhanced permeability and retention (EPR) effects; what is the appropriate target?. *Theranostics* **2014**, *4*, 81-89.
4. Shi, J.; Kantoff, P. W.; Wooster, R. Farokhzad, O. C. Cancer nanomedicine: progress, challenges and opportunities. *Nat. Rev. Cancer* **2017**, *17*, 20-37.

5. Stewart, M. P.; Sharei, A.; Ding, X. Y.; Sahay, G.; Langer, R.; Jensen, K. F. *In vitro* and *ex vivo* strategies for intracellular delivery. *Nature* **2016**, *7624*, 183-192.

6. Xu, Z.; Ma, X.; Gao, Y.; Hou, M.; Xue, P.; Li, C. M.; Kang, Y. Multifunctional silica nanoparticles as a promising theranostic platform for biomedical applications. *Mater. Chem. Front.* **2017**, *1*, 1257-1272.

7. Chen, G. Y.; Roy, I.; Yang, C. H.; Prasad, P. N. Nanochemistry and nanomedicine for nanoparticle-based diagnostics and therapy. *Chem. Rev.* **2016**, *5*, 2826-2885

8. Su, H.; Koo, J. M.; Cui, H. G. One-component nanomedicine. *J. Control. Release* **2015**, *219*, 383–395

9. Barenholz, Y. Doxil® −The first FDA-approved nano-drug: Lessons learned. *J. Control. Release* **2012**, *160*, 117-134

10. Pattni, B. S.; Chupin, V. V.; Torchilin, V. P. New developments in liposomal drug delivery. *Chem. Rev.* **2015**, *115*, 10938-10966

11. Li, Y. L.; Maciel, D.; Rodrigues, J.; Shi, X. Y.; Tomás, H. Biodegradable polymer nanogels for drug/nucleic acid delivery. *Chem. Rev.* **2015**, *115*, 8564-8608

12. Wang, H.; Huang, Q.; Chang, H.; Xiao, J. R.; Cheng, Y. Y. Stimuli-responsive dendrimers in drug delivery. *Biomater. Sci.* **2016**, *4*, 375–390.

13. Sun, C. Y.; Liu, Y.; Du, J. Z.; Cao, Z. T.; Xu, C. F.; Wang, J. Facile generation of tumor ph-labile linkage-bridged block copolymer for expeditious chemotherapeutic delivery. *Angew. Chem. Int. Ed.* **2016**, *55*, 1010 -1014.

14. Shin, W. S.; Han, J. Y.; Verwilst, P.; Kumar, R.; Kim, J.-H.; Kim, J. S. Cancer targeted enzymatic theranostic prodrug: precise diagnosis and chemotherapy. *Bioconjugate Chem*. **2016**, *27*, 1419−1426.

15. Xu, Z. G.; Liu, S. Y.; Kang, Y. J.; Wang, M. F. Glutathione-responsive polymeric micelles formed by a biodegradable amphiphilic triblock copolymer for anticancer drug delivery and controlled release. *ACS Biomater. Sci. Eng.* **2015**, *1*, 585−592.

16. Li, H. J.; Du, J. Z.; Du, X. J.; Xu, C. F.; Sun, C. Y.; Wang, H. X.; Cao, Z. T.; Yang, X. Z.; Zhu, Y.H.; Nie, S.M.; Wang, J. Stimuli-responsive clustered nanoparticles for improved tumor penetration and therapeutic efficacy. *Proc. Natl. Acad. Sci. U. S. A.* **2016**, *15*, 4164-4169.

17. Wei, H.; Zhuo, R. X.; Zhang, X. Z. Design and development of polymeric micelles with cleavable links for intracellular drug delivery. *Prog. Polym. Sci.* **2013**, *38*, 503- 535.

18. Xu, Z. G.; Liu, S. Y.; Kang, Y. J.; Wang, M. F. Glutathione- and pH-responsive nonporous silica prodrug nanoparticles for controlled release and cancer therapy. *Nanoscale* **2015**, *7*, 5859-5868.

19. Mao, J.; Li, Y.; Wu, T.; Yuan, C. H.; Zeng, B. R.; Xu, Y. T.; Dai, L. Z. A simple dual-pH responsive prodrug-based polymeric micelles for drug delivery. *ACS Appl. Mater. Interfaces* **2016**, *8*, 17109−17117.

20. Wang, Y.; Wei, G. Q.; Zhang, X. B.; Xu, F. N.; Xiong, X.; Zhou, S. B. A step-by-step multiple stimuli-responsive nanoplatform for enhancing combined chemo-photodynamic therapy. *Adv. Mater.* **2017**, *29*, 1605357

21. Jia, T.; Huang, S.; Yang C. J.; Wang, M. F. Unimolecular micelles of amphiphilic cyclodextrin-core star-like copolymers with covalent pH-responsive linkage of anticancer prodrugs. *Mol. Pharmaceutics* **2016**, *14*, 2529-2537.

22. Yoshii, T.; Mizusawa, K.; Takaoka, Y.; Hamachi, I. Intracellular protein-responsive supramolecules: protein sensing and in-cell construction of inhibitor assay system. *J. Am. Chem. Soc.* **2014**, *136*, 16635–16642.

23. Liu, G.; Gao, H. J.; Zuo, Y. X.; Zeng, X. W.; Tao, W.; Tsai, H.; Mei, L. DACHPt-loaded unimolecular micelles based on hydrophilic dendritic block copolymers for enhanced therapy of lung cancer. *ACS Appl. Mater. Interfaces* **2017**, *9*, 112-119.

24. Sun, P.; Chen, D.; Deng, H.; Wang, N.; Huang, P.; Jin, X.; Zhu, X. "Bottom-up" construction of multi-polyprodrug-arm hyperbranched amphiphiles for cancer therapy. *Bioconjugate Chem.* **2017**, *28*, 1470-1480.

25. Fan, X.; Wang, Z.; He, C. "Breathing" unimolecular micelles based on a novel star-like amphiphilic hybrid copolymer. *J. Mater. Chem. B* **2015**, *3*, 4715-4722.

26. Chen, G.; Shi, X.; Wang, B.; Xie, R.; Guo, L. W.; Gong, S.; Kent, K. C. Unimolecular micelle-based hybrid system for perivascular drug delivery produces long-term efficacy for neointima attenuation in rats. *Biomacromolecules* **2017**, *18*, 2205–2213.

27. Ren, J. M.; McKenzie, T. G.; Fu, Q.; Wong, E. H. H.; Xu, J.T.; An, Z.S.; Shanmugam, S.; Davis, T.P.; Boyer C. and Qiao, G.G. Star polymers. *Chem. Rev.* **2016**, *116*, 6743-6836.

28. Fan, X. S.; Li, Z. B.; Loh, X. J. Recent development of unimolecular micelles as functional materials and applications. *Polym. Chem.* **2016**, *7*, 5898-5919.

29. Wei, H.; Wang, C. E.; Tan, N.; Boydston, A. J.; Pun, S. H. ATRP Synthesis of Sunflower Polymers using Cyclic Multimacroinitiator. *ACS Macro Lett.* **2015**, *9*, 938-941.

30. Xin, P. Y.; Tan, S.; Sun, Y. H.; Ren, Q.; Dong, W. P.; Guo, J. J.; Jiang, T.; Chen, C. P. One-pot formation of hydrazide macrocycles with modified cavities: an example of pH-sensitive unimolecular cation channels. *Chem. Commun.* **2017**, *53*, 5322-5325.

31. Wang, C. E.; Wei, H.; Tan, N.; Boydston, A. J.; Pun, S. H. Sunflower Polymers for Folate-Mediated Drug Delivery. *Biomacromolecules* **2016**, *17*, 69-75.

32. Hu, X.; liu, G.; Li, Y.; Wang, X.; Liu, S. Cell-penetrating hyperbranched polyprodrug amphiphiles for synergistic reductive milieu-triggered drug release and enhanced magnetic resonance signals. *J. Am. Chem. Soc.* **2015**, *137*, 362-368.

33. Huang, Y.; Qiu, F.; Shen, L.; Chen, D.; Su, Y.; Yang, C.; Li, B.; Yan, D.; Zhu, X. Combining two-photon-activated fluorescence resonance energy transfer and near-infrared photothermal effect of unimolecular micelles for enhanced photodynamic therapy. *ACS Nano* **2016**, *10*, 10489-10499.

34. Kurniasih, I. N.; Keilitz, J.; Haag, R. Dendritic nanocarriers based on hyperbranched polymers. *Chem. Soc. Rev.* **2015**, *44*, 4145-4164.

35. Pang, X. C.; Zhao, L.; Feng, C. W.; Lin, Z. Q. Novel amphiphilic multiarm, starlike coilrod diblock copolymers *via* a combination of click chemistry with living polymerization. *Macromolecules* **2011**, *44*, 7176-7183.

36. Xu, Z. G.; Liu, S. Y.; Liu, H.; Yang, C. J.; Kang, Y. J.; Wang, M. F. Unimolecular micelles of amphiphilic cyclodextrin-core star-like block copolymers for anticancer drug delivery. *Chem. Commun.* **2015**, *51*, 15768-15771.

37. Shi, X. X.; Ma X. Q.; Hou, M. L.; Gao, Y. E.; Bai, S.; Xiao, B.; Xue, P.; Kang, Y. J.; Xu, Z. G.; Li C. M. pH-Responsive unimolecular micelles based on amphiphilic star-

like copolymers with high drug loading for effective drug delivery and cellular imaging. *J. Mater. Chem. B* **2017**, *5*, 6847-6859.

38. Yang, C. J.; Huang, S.; Wang, X.; Wang, M. F. Theranostic Unimolecular Micelles of Highly Fluorescent Conjugated Polymer Bottlebrushes for Far Red/Near Infrared Bioimaging and Efficient Anticancer Drug Delivery. *Polym. Chem.* **2016**, *7*, 7455-7468.
39. Qiu, L.; Liu, Q.; Hong, C.-Y.; Pan, C.-Y. Unimolecular micelles of camptothecin-bonded hyperbranched star copolymers *via* b-thiopropionate linkage: synthesis and drug delivery. *J. Mater. Chem. B* **2016**, *4*, 141-151.
40. Wang, H.; Xu, F.; Li, D.; Liu, X.; Jin, Q.; Ji, J. Bioinspired phospholipid polymer prodrug as a pH-responsive drug delivery system for cancer therapy. *Polym. Chem.* **2013**, *4*, 2004-2010.
41. Pang, X. C.; Zhao, L.; Han, W.; Xin, X. K.; Lin, Z. Q. A general and robust strategy for the synthesis of nearly monodisperse colloidal nanocrystals. *Nat. Nanotechnol.* **2013**, *8*, 426−431.
42. Xu, Z. G.; Zhang, K. L.; Hou, C. L.; Wang, D. D.; Liu, X. Y.; Guan, X. J.; Zhang, X. Y.; Zhang, H. X. A novel nanoassembled doxorubicin prodrug with a high drug loading for anticancer drug delivery. *J. Mater. Chem. B* **2014**, *2*, 3433-3437.
43. Rui, M.; Xin, Y.; Li, R.; Ge, Y.; Feng, C.; Xu, X.; Targeted biomimetic nanoparticles for synergistic combination chemotherapy of paclitaxel and doxorubicin, *Mol. Pharmaceutics* **2017**, *14*, 107-123.
44. Mai, Y.; Eisenberg, A. Self-assembly of block copolymers. *Chem. Soc. Rev.* **2012**, *41*, 5969-5985.

45. Xu, Z. G.; Shi, X. X.; Hou, M. L.; Xue, P.; Gao, Y. E.; Liu, S. Y.; Kang, Y. J. Disassembly of amphiphilic small molecular prodrug with fluorescence switch induced by pH and folic acid receptors for targeted delivery and controlled release. *Colloid. Surface. B* **2017**, *150*, 50-58.

46. Wang, Y.G.; Zhou, K. J.; Huang, G.; Hensley, C.; Huang, X. N.; Ma, X. P.; Zhao, T.; Sumer, B. D.; DeBerardinis R. J.; Gao, J. M. A nanoparticle-based strategy for the imaging of a broad range of tumours by nonlinear amplification of microenvironment signals. *Nat. Mater.* **2014**, *2*, 204-212.

47. Wang, Y.; Zheng, J.; Tian Y.; Yang, W. Acid degradable poly(vinylcaprolactam)-based nanogels with ketal linkages for drug delivery. *J. Mater. Chem. B* **2015**, *3*, 5824–5832.

48. Cheng, R.; Zou, R.; Ou, S.; Guo, R.; Yan, R.; Shi, H.; Yu, S.; Li, X.; Bu Y.; Lin, M. Graphene oxide complex as a pH-sensitive antitumor drug. *Polym. Chem.* **2015**, *6*, 2401–2406.

49. Zhang, X.; Zhang, H.; Liang, X.; Zhang, J.; Zhang, X.; Tao, W.; Zhu, X.; Chang, D.; Zeng, X.; Liu, G.; Mei, L. Iron oxide nanoparticles induce autophagosome accumulation through multiple mechanisms: lysosome impairment, mitochondrial damage, and ER stress. *Mol. Pharmaceutics* **2016**, *13*, 2578-2587.

Table of Content Graphic

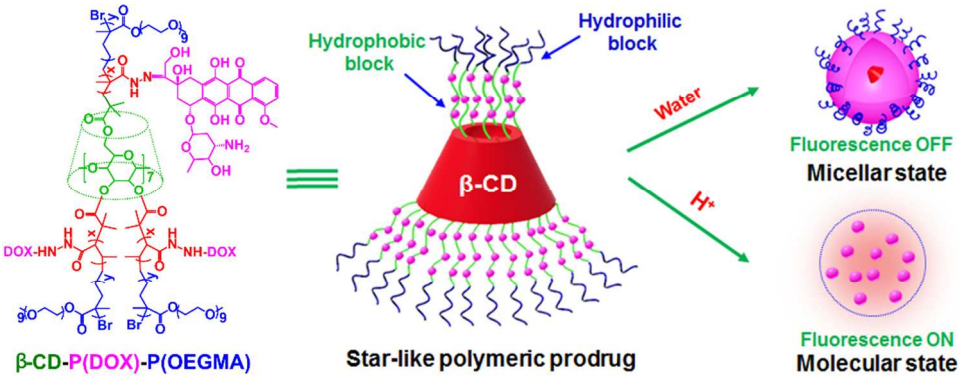

Theranostic nanoplatform based on acid-responsive star-like polymeric prodrug with high drug loading content for enhanced anti-tumor efficacy.

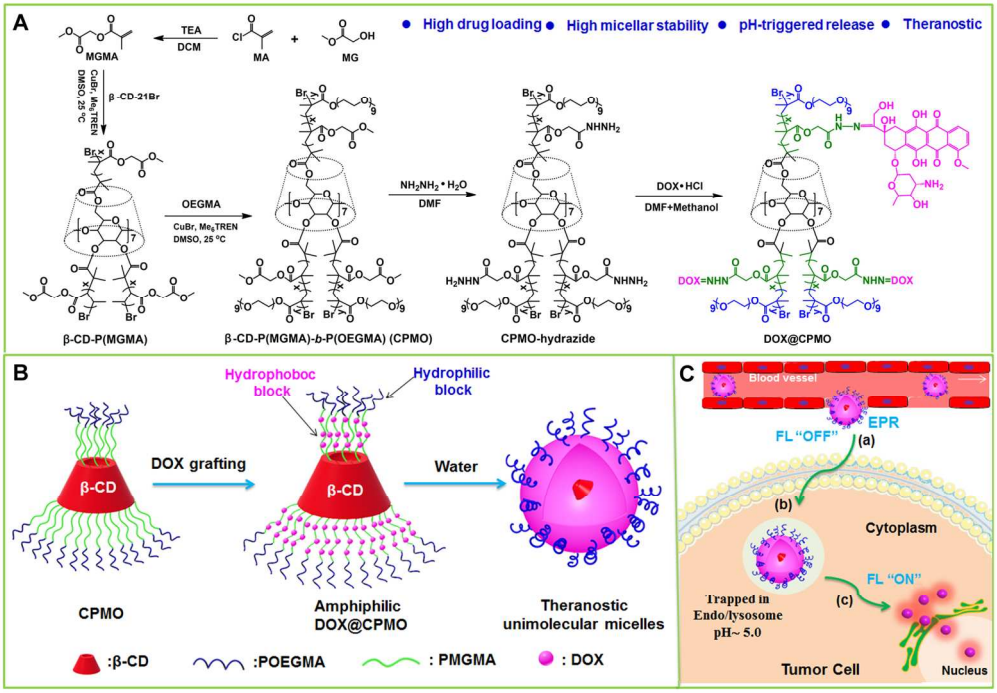

Scheme 1. (A) The synthetic route of DOX@CPMO polymeric prodrug. (B) Schematic diagram of DOX@CPMO as a theranostic platform for cancer therapy. (C) The enhanced permeability and retention (EPR) effect-mediated cell endocytosis and fluorescence (FL) ON-OFF process: (a) The DOX@CPMO UMs entering a tumor cell mediated by EPR effect (FL-OFF); (b) DOX@CPMO UMs were trapped in endo/lysosomes; (c) DOX was delivered into nucleus by pH-triggered release (FL-ON), realizing theranostic functionality of UMs.

160x111mm (300 x 300 DPI)

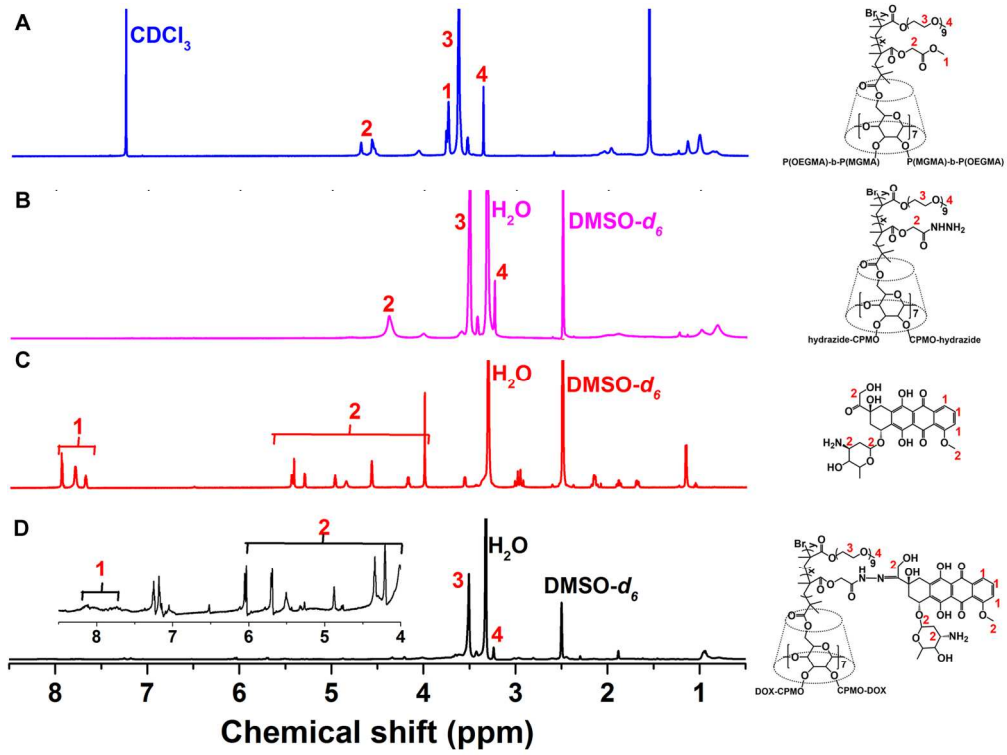

Figure 1. 1H NMR spectra in CDCl3 or DMSO-d6 of (A) β-CD-P(MGMA)18-b-P(OEGMA)5 (CPMO-1) , (B) CPMO-1 hydrazide, (C) free DOX and (D) DOX@CPMO-1 prodrug.

160x120mm (300 x 300 DPI)

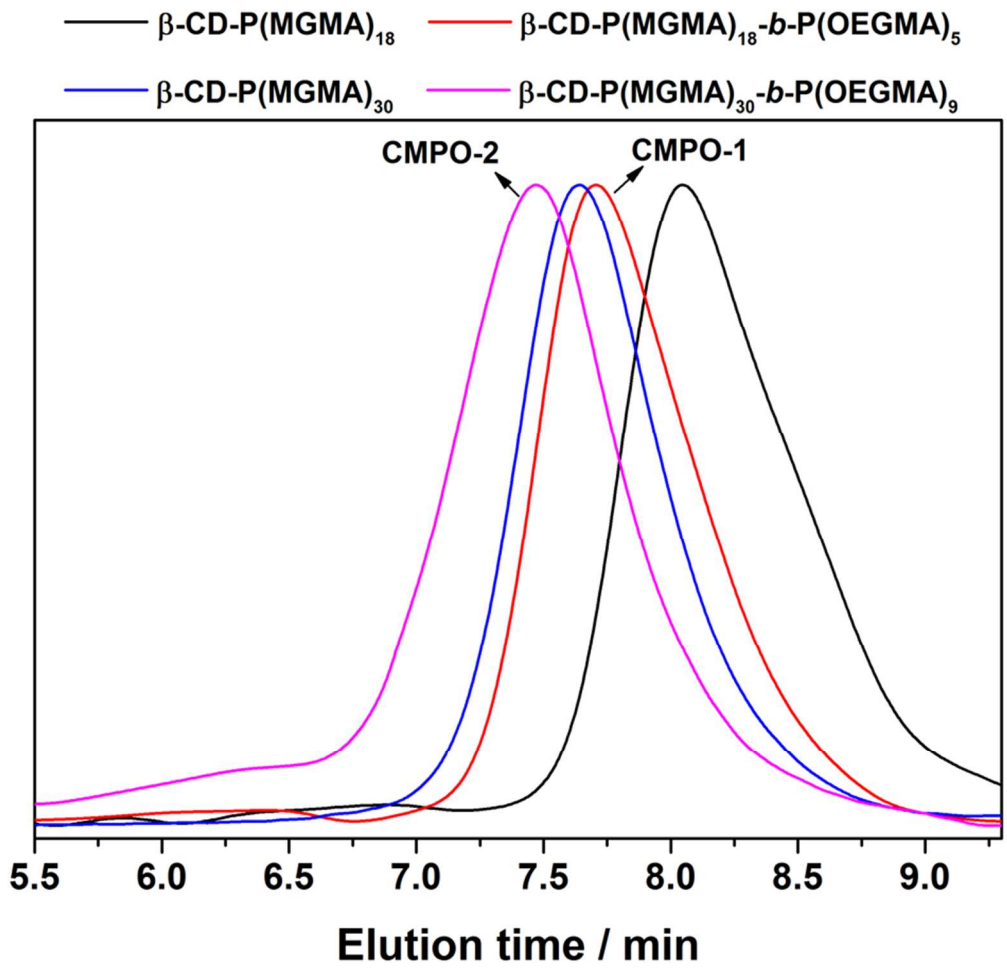

Figure 2. The GPC chromatograms of star-like CPMO diblock copolymer and their previous product in THF.

80x76mm (300 x 300 DPI)

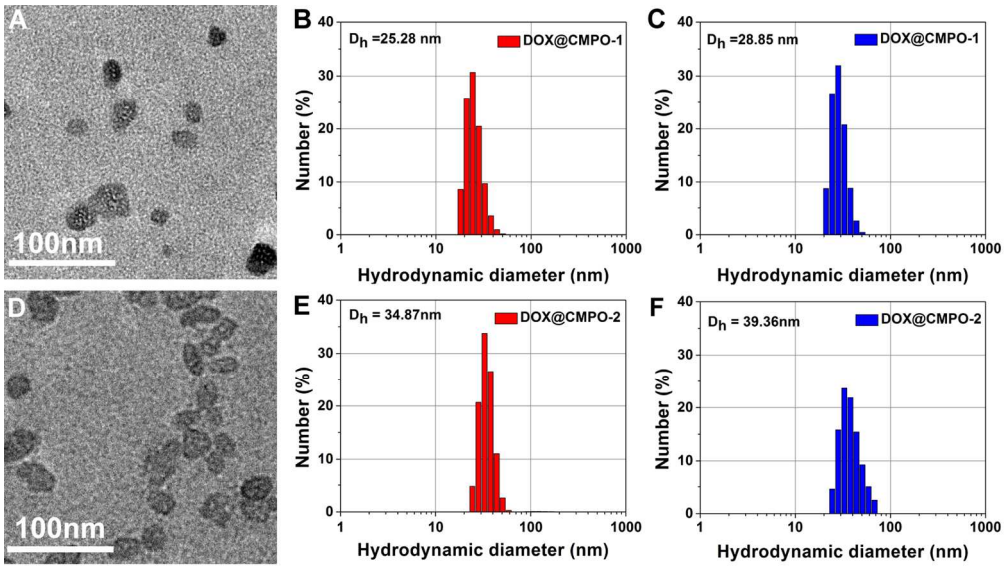

Figure 3. TEM images of DOX@CPMO-1 (A) and DOX@CPMO-2 (D) UMs; The DLS histograms of DOX@CPMO-1 and DOX@CPMO-2 UMs in water (B and E) and DMF solvent (C and F).

146x82mm (300 x 300 DPI)

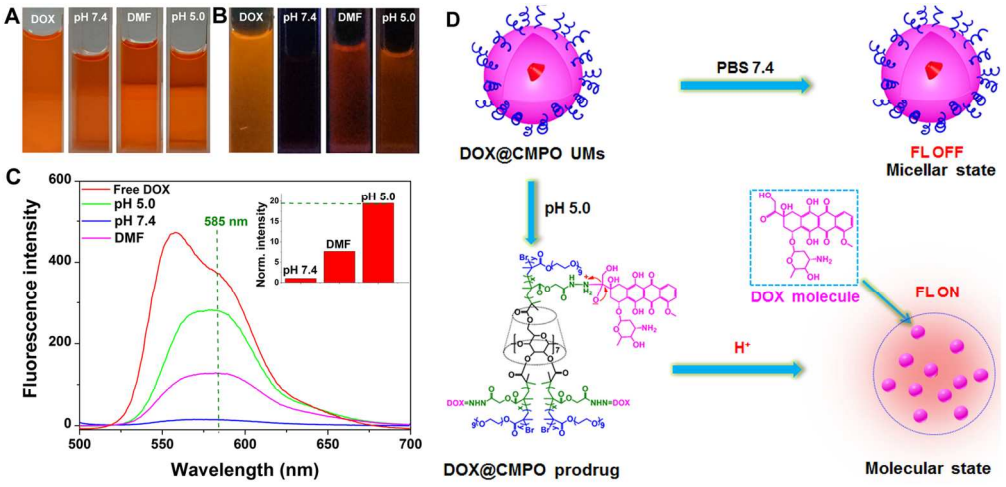

Figure 4. The images of free DOX and different DOX@CPMO-1 solutions under (A) visible light and (B) UV irradiation (365 nm); (C) The fluorescence emission spectra of different DOX@CPMO-1micelles (λexc = 488 nm) and the inset histogram shows the normalized fluorescence intensity of different DOX@CPMO-1 solutions; (D) The proposed mechanism leading to the pH-triggered DOX release and pH-depending enhanced fluorescence intensity.

157x76mm (300 x 300 DPI)

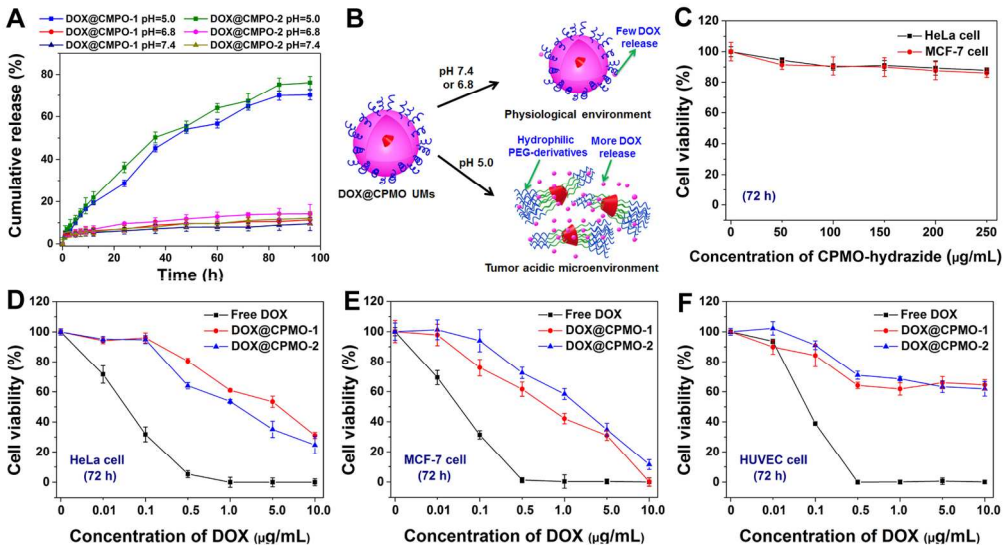

Figure 5. (A) DOX release from DOX@CPMO UMs in different PBS solutions (pH 7.4, 6.8 or 5.0) for 96 h at 37 °C. (B) The schematic diagram of drug release in different pH conditions. (C) Viability of HeLa and MCF-7 cells cultured with CPMO-hydrazide blank micelles for 72 h. (D-F) The viability of HeLa cells (D), MCF-7 cells (E) and HUVEC cells (F) incubated with free DOX, DOX@CPMO-1and DOX@CPMO-2 under various DOX concentrations for 72 h. All the data are presented as means ± SD (n = 3).

160x86mm (300 x 300 DPI)

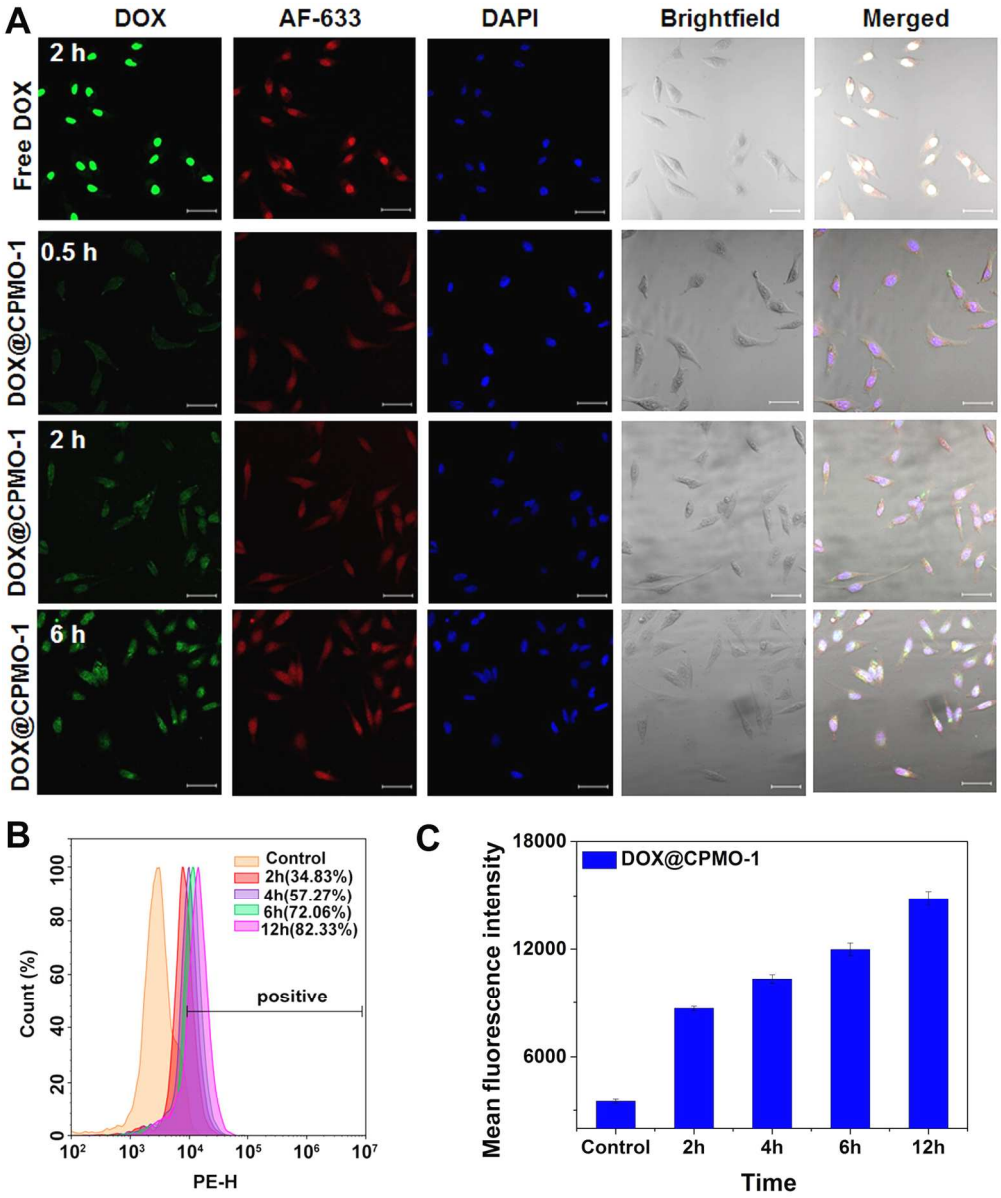

Figure 6. (A) CLSM and bright field images of HeLa cells incubated with free DOX or DOX@CPMO-1 micelles. (Equivalent DOX concentration: 20 μg/mL). The fluorescence of DOX, AF-633 and DAPI were pseudo-labeled as green, red and blue, respectively. Scale bars: 50 μm. (B) Flow cytometry analysis of the intracellular uptake of DOX@CPMO-1 micelles in HeLa cells treated for 0, 2, 4, 6 and 12 h; (C) Mean fluorescence intensity of DOX@CPMO-1 micelles at different time points. The data were presented as the mean ± SD (n=3).

160x190mm (300 x 300 DPI)

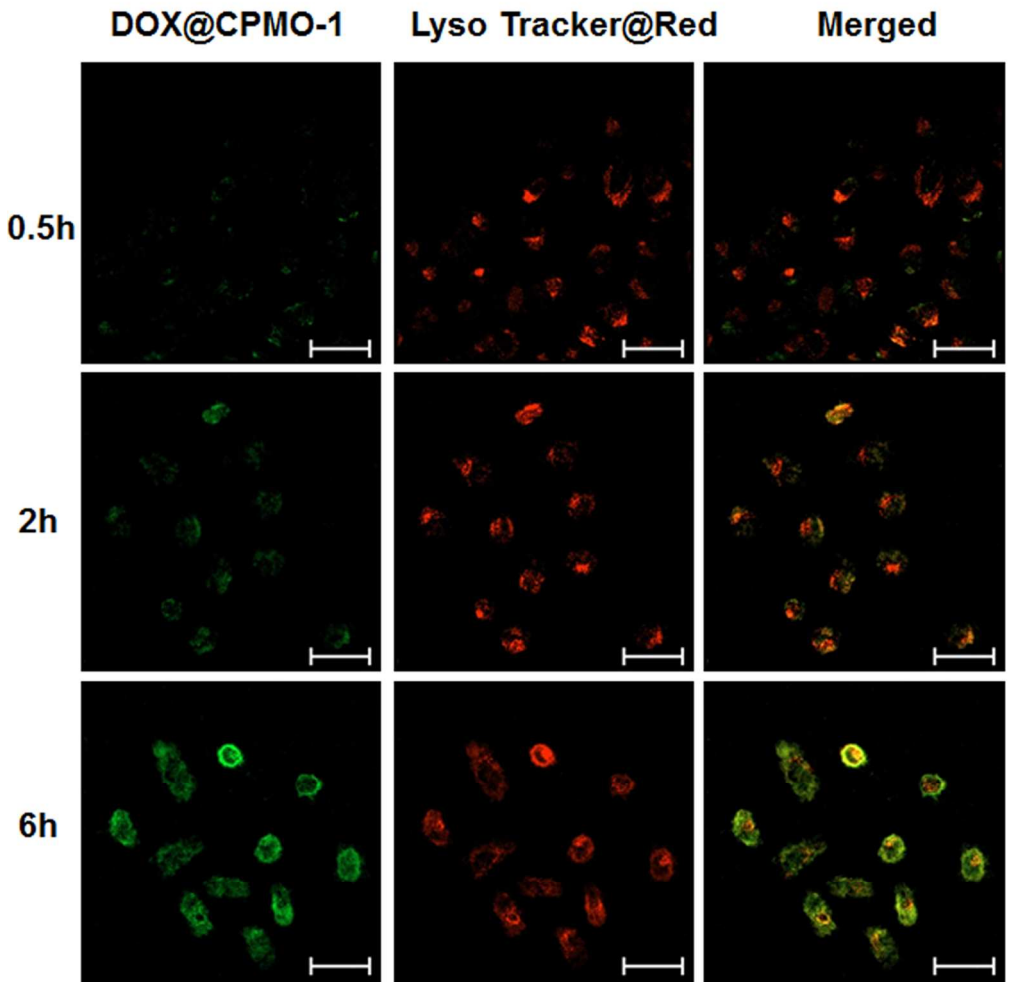

Figure 7. (A) CLSM images of HeLa cells after incubation with DOX@CPMO-1 micelles for 0.5, 2 and 6 h (equivalent DOX concentration: 20 μg/mL). The fluorescence of DOX, Lyso Tracker@Red was labeled as green and red, respectively. Scale bars: 50 μm.

119x118mm (300 x 300 DPI)